nature COMMUNICATIONS

Corrected: Author correction

ARTICLE

DOI: 10.1038/s41467-018-03015-3 OPEN

Direct measurement of superdiffusive energy transport in disordered granular chains

Eunho Kim [1,2], Alejandro J. Martínez[3], Sean E. Phenisee[1], P.G. Kevrekidis[4], Mason A. Porter [3,5,6] & Jinkyu Yang[1]

Energy transport properties in heterogeneous materials have attracted scientific interest for more than half of a century, and they continue to offer fundamental and rich questions. One of the outstanding challenges is to extend Anderson theory for uncorrelated and fully disordered lattices in condensed-matter systems to physical settings in which additional effects compete with disorder. Here we present the first systematic experimental study of energy transport and localization properties in simultaneously disordered and nonlinear granular crystals. In line with prior theoretical studies, we observe in our experiments that disorder and nonlinearity—which individually favor energy localization—can effectively cancel each other out, resulting in the destruction of wave localization. We also show that the combined effect of disorder and nonlinearity can enable manipulation of energy transport speed in granular crystals. Specifically, we experimentally demonstrate superdiffusive transport. Furthermore, our numerical computations suggest that subdiffusive transport should be attainable by controlling the strength of the system's external precompression force.

[1] Department of Aeronautics and Astronautics, University of Washington, Seattle, WA 98195-2400, USA. [2] Division of Mechanical System Engineering & Automotive Hi-Technology Research Center, Chonbuk National University, 567 Baekje-daero, Deokjin-gu, Jeonju-si, Jeollabuk-do, 54896, Republic of Korea. [3] Oxford Centre for Industrial and Applied Mathematics, Mathematical Institute, University of Oxford, Oxford, OX2 6GG, UK. [4] Department of Mathematics and Statistics, University of Massachusetts, Amherst, MA 01003-4515, USA. [5] Department of Mathematics, University of California, Los Angeles, CA 90095, USA. [6] CABDyN Complexity Centre, University of Oxford, Oxford, OX1 1HP, UK. Eunho Kim and Alejandro J. Martínez contributed equally to this work. Correspondence and requests for materials should be addressed to M.A.P. (email: mason@math.ucla.edu)

P. W. Anderson's 1958 paper[1] on wave dynamics in disordered systems is one of the landmarks of 20th-century physics, and studies of Anderson localization and related phenomena continue to yield fascinating surprises[2]. Over the past decade, there have been amazing experimental advances, in fields such as ultracold atomic physics and nonlinear optics, toward the direct observation of spatial localization and transport in disordered systems[3–5]. There has been simultaneous progress toward achieving a theoretical understanding of the interplay between disorder and weak nonlinearity[6]. However, there has been much less exploration of disorder in strongly nonlinear systems, and many fundamental questions remain open. Specifically, under what conditions is transport subdiffusive or superdiffusive? More generally, how does strong nonlinearity affect localization? Much of the progress has arisen from studies of models with on-site nonlinearities, such as discrete nonlinear Schrödinger and Klein–Gordon models, where the interplay between disorder and nonlinearity yields subdiffusive transport[6–8]. However, recent progress has hinted at a fundamentally different phenomenology in lattices with inter-site interactions (e.g., well-known settings such as chains of Fermi–Pasta–Ulam–Tsingou (FPUT) type[9,10]). In particular, it has been shown numerically that superdiffusive behavior is possible in these systems[11–13]. An intriguing feature in all of the above situations is that disorder (which is traditionally viewed as leading to localization) and nonlinearity (which can cause localization in the form of phenomena such as discrete breathers[14]) can somehow cancel out each other's tendency toward localization, leading to transport.

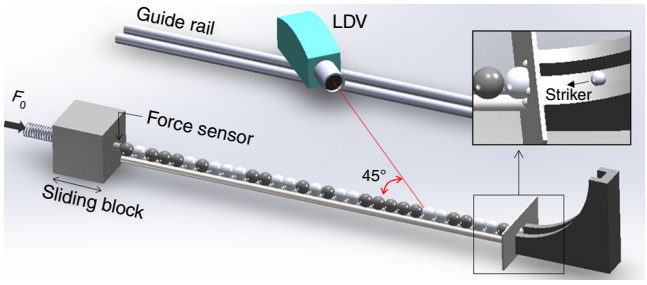

Fig. 1 Schematic of our experimental setup. The inset shows details of the boundary condition in front of a granular chain

In this study, we experimentally and numerically investigate energy transport in one-dimensional disordered granular crystals (i.e., granular chains) in a wide variety of regimes, extending from almost linear to strongly nonlinear ones. Granular crystals composed of spherical particles are a popular vehicle for investigating various nonlinear wave features[15–18]. When in contact, two particles interact with each other nonlinearly via a Hertzian interaction[19]: the force–displacement relation in the contact interaction is governed by a 3/2 power law under compression and zero force under tension. In this class of models, one can tune the effective system nonlinearity very precisely by varying the ratio of excitation amplitude to static precompression[18]. We consider a system excited at a granular chain's boundary to investigate how the mechanical energy injected by the external excitation is transported along the chain under the combined influence of nonlinearity and disorder. In our analysis, we use established diagnostics such as the inverse participation ratio (IPR) and the second moment (m_2) of the energy[6]. Earlier works have used such quantities to characterize transport in homogeneous, tapered, and diatomic granular chains[20], as well as in disordered granular chains[11,12]. A very recent study examined the relation between chaos and transport properties in granular chains[21].

Results

Experimental setup and data. We describe our experimental setup in Fig. 1. The granular chain consists of 32 spherical particles (see Supplementary Table 1 and Supplementary Note 1). To introduce disorder in a granular crystal, we use various combinations of aluminum and tungsten-carbide particles, which have starkly different densities and elastic moduli (see the Methods section for details). The right end of the chain is constrained by a steel plate with a hole in the center; through this hole, a spherical impactor released from a ramp hits and excites the first particle of the chain. The left end of the chain is blocked by a large sliding mass, which applies a static precompression F_0 to the chain via a linear spring. We measure the dynamics of the chain by recording each particle's velocity as a function of time using a laser Doppler vibrometer (LDV)[22].

We control the strength of the system's nonlinearity by applying three different amounts of precompression: 50, 10, and 0 N, which range from almost linear to strongly nonlinear

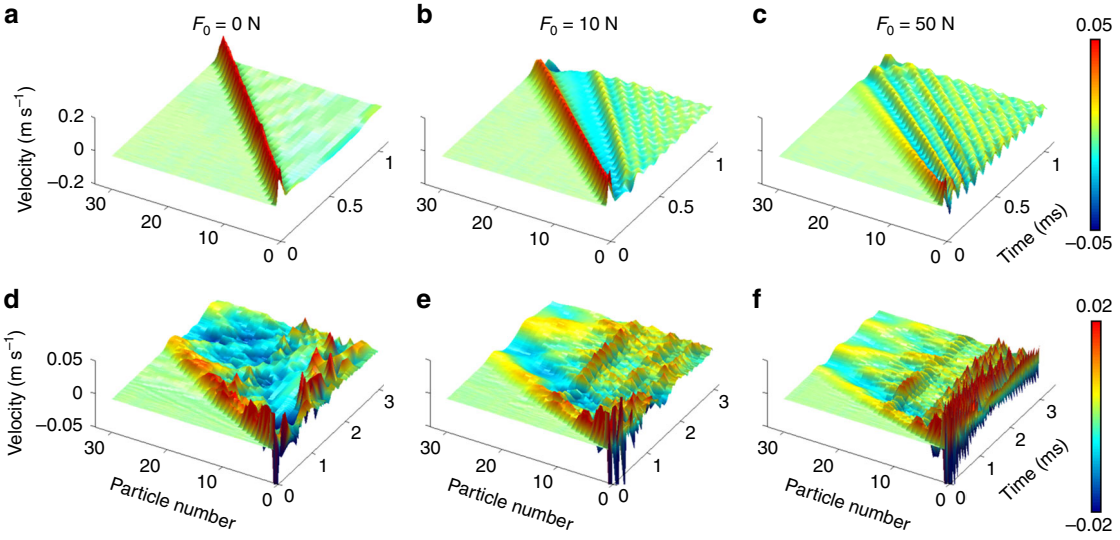

Fig. 2 Wave propagation in homogeneous and disordered chains. Spatiotemporal distributions of particle velocities in (**a**–**c**) a homogeneous chain and (**d**–**f**) a disordered chain with static precompressions of (**a**, **d**) 0 N, (**b**, **e**) 10 N, and (**c**, **f**) 50 N

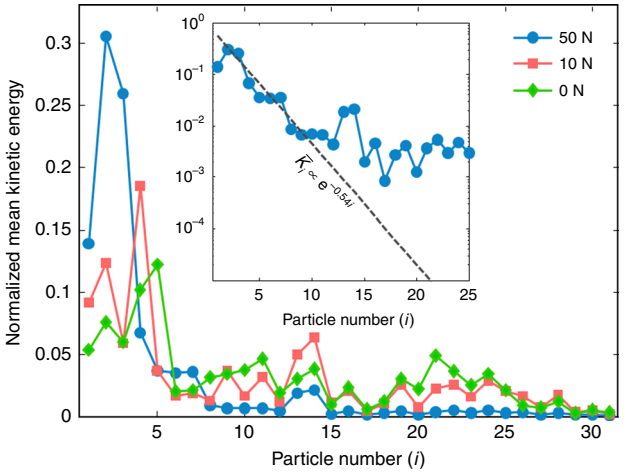

Fig. 3 Experimental observation of Anderson-like localization. Normalized kinetic-energy profile, averaged between 1.5 and 3.5 ms, for different amounts of precompression. In the inset, we show the kinetic energy on a logarithmic scale when the static precompression is 50 N. The dashed line shows the slope associated with $e^{-0.54i}$, where i denotes particle number

dynamical regimes of the chain. To visualize the propagation of stress waves in each case, we show spatiotemporal distributions of the particles' motions based on the measured velocity. In Fig. 2, we show experimental measurements of particle velocities for a homogeneous chain consisting of (top row) aluminum particles only and (bottom row) a disordered chain composed of aluminum and tungsten-carbide particles in strongly nonlinear, weakly nonlinear, and almost linear scenarios (left, middle, and right, respectively). See Supplementary Fig. 1 and Supplementary Note 2 for details of how we characterize nonlinearity strength.

In a homogeneous chain, we observe a localized wave packet in the form of a strongly nonlinear solitary wave in the absence of precompression (i.e., for $F_0 = 0$ N). When we apply a nonzero precompression to the chain, we start to observe the generation of linear oscillatory waves, which propagate behind the supersonic leading nonlinear wave packet. These ripples arise from oscillations of the first particle after an impact[23] and consequently from the excitation of oscillatory modes. The frequency of these oscillatory waves increases as the precompression increases (compare Figs 2b and 2c). This occurs because the contact stiffness increases as we apply progressively stronger precompression due to the nonlinearity in the contact interactions.

In Figs 2d–f, we show experimental results for wave propagation in a disordered chain for various precompression strengths. (See Supplementary Table 1 and Supplementary Note 1 for details of the disordered chain configuration, Supplementary Fig. 2 and Supplementary Note 1 for our comparison with simulation results, and Supplementary Fig. 3 and Supplementary Note 3 for a corresponding frequency analysis.) Comparing our results for disordered chains with the ones from the homogeneous chain, we find that the presence of disorder causes significant scattering of propagating waves in both time and space. The scattering is most drastic in the absence of precompression (see Fig. 2d). However, for increasing precompression, the wave packet tends to become more localized in the front of the chain and the amplitudes of propagating waves decrease significantly as a function of distance (see Fig. 2f). Given identical excitation conditions, we observe that applying precompression increases the speed of the leading wave packet, as expected in granular chains due to the dependence of the wave speed on wave amplitude and chain stiffness (i.e., precompression)[15–18].

Experimental observation of Anderson-like localization. To characterize localization near the excitation point in the almost linear regime (i.e., $F_0 = 50$ N), we compute the kinetic-energy distribution. Given the velocity $v_i(t)$ of the i^{th} particle, we compute its kinetic energy $K_i(t) = (1/2)m_i v_i^2(t)$, where m_i is the particle's mass. We then average our results over the different realizations of disorder to obtain $\langle K_i(t)\rangle$. Initially, the pattern's amplitude decreases due to the spreading associated with non-scattered modes. It then oscillates near the edge of the chain for a long time (up to 3.5 ms). To better visualize the kinetic-energy profile, we compute a temporal mean between $t_s = 1.5$ ms and $t_f = 3.5$ ms. We define the mean kinetic energy as $\overline{K}_i = \int_{t_s}^{t_f} \langle K_i(t)\rangle \mathrm{d}t/(t_f - t_s)$, and we then normalize the distribution by letting $\overline{K}_i \to \overline{K}_i / \sum_{j=1}^{N} \overline{K}_j$ (where N is the number of particles). In Fig. 3, we show normalized mean kinetic-energy profiles for the different precompression strengths. In our experiments, we observe for $F_0 = 50$ N that the kinetic-energy distribution seems at first to decay at a roughly exponential rate with particle number: $\overline{K}_i \propto e^{-0.54i}$ for $i \in \{2,\ldots,10\}$. (See the inset of Fig. 3 and Supplementary Note 4 for more details.) Due to this exponential decay, the kinetic energy is reduced by two orders of magnitude after about 10 sites from the boundary of the chain. We also observe localization around the second particle. This particular location arises from a combination of dissipation effects and the particular disordered configurations (from a sub-ensemble in which the first particle is always aluminum) that we examine. For $i \in \{11, \ldots,15\}$, we observe excitation of a secondary mode that emerges and decays in an irregular manner as a function of time (see Fig. 3). For $i \gtrsim 15$, very low-amplitude waves, which are associated primarily with low-frequency linear modes, reach the right side of the chain and are reflected.

Energy localization and spreading. To investigate the energy transport characteristics of the granular chains, we quantify energy localization and the speed of energy spreading using the inverse participation ratio (IPR) and the second moment of the energy (m_2), respectively[6,11,24]. To calculate these quantities, we use kinetic energy instead of the total energy of the particles in a chain, because we can directly calculate the former experimentally by measuring particle velocities. The IPR based on the kinetic energy is

$$P^{-1}(t) = \frac{\sum_{i=1}^{N} \left(m_i v_i^2\right)^2}{\left(\sum_{i=1}^{N} m_i v_i^2\right)^2}. \quad (1)$$

When all energy is confined to a single particle, $P^{-1} = 1$, and P^{-1} approaches $1/N$ (where N is the total number of particles in a chain) as a wave disperses. In Fig. 4, we show P^{-1} as a function of time for both the almost linear and nonlinear regimes. Because of the customary exchange between kinetic and potential energies, we observe oscillations in the temporal profile of P^{-1}. However, the aggregate trends do not vary significantly from those based on total energy (see Supplementary Fig. 4 and Supplementary Note 5).

In a homogeneous chain with precompression (see the solid blue curve in Fig. 4a), we observe experimentally that P^{-1} decreases in time, because the linear waves disperse as they propagate. However, in a disordered chain (see the solid red curve in Fig. 4a), this decreasing trend is less pronounced. This implies that the disorder tends to favor wave localization, confirming the effect of Anderson localization. Our numerical simulations (dashed curves; see the Methods section) corroborate our

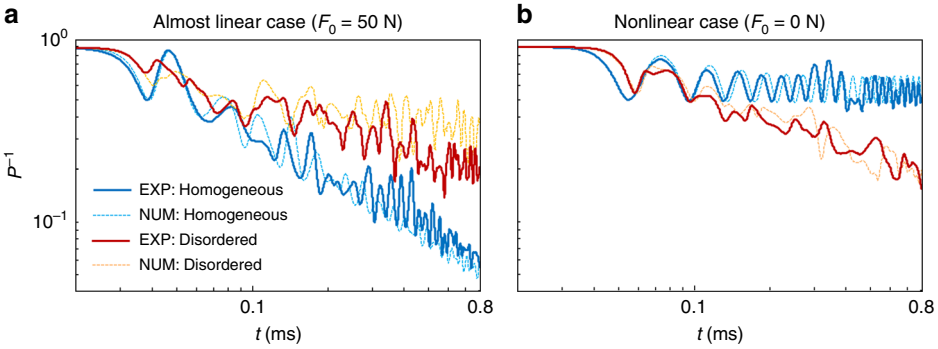

Fig. 4 Energy-localization characteristics. Inverse participation ratio (P^{-1}) of the kinetic energy in homogeneous (blue curves) and disordered (red curves) chains for (**a**) almost linear and (**b**) nonlinear regimes. In both cases, we compare numerical calculations (dashed curves) with experimental data (solid curves)

experimental results. Strikingly, we observe completely different qualitative behavior in the nonlinear regime (see Fig. 4b). The nonlinearity favors wave localization in a homogeneous chain, as indicated by the larger value of P^{-1}. In this case, a localized solitary wave propagates in a highly localized (doubly exponentially decaying[25]) manner, and P^{-1} retains a value of about 0.6. A similar trend was noted recently in numerical simulations[11,12] for bulk dynamics in very long chains (so boundary effects were neglected). In contrast, in our experiments, boundary effects are fundamental both for the generation of the initial excitation and for the ensuing dynamics.

The second moment of kinetic-energy distribution is

$$m_2(t) = \frac{\sum_{i=1}^{N} i^2 \left(m_i v_i^2\right)}{\sum_{i=1}^{N} m_i v_i^2}. \qquad (2)$$

It is well-known that asymptotic energy spreading in a homogeneous chain is ballistic (i.e., $m_2(t) \sim t^2$ as $t \to \infty$)[11,26]. To investigate energy spreading in detail, we estimate the exponent γ of the second moment in the scaling relationship $m_2(t) \sim t^\gamma$ during the time period from 0.1 ms to 1 ms[6,11,12]. We compare the estimated exponents from the experimental data to those from numerical simulations in Fig. 5. The exponents in homogeneous chains (see the upper shaded area in Fig. 5) are about $\gamma = 2$ (corresponding to ballistic spreading). For stronger precompression, the exponents are slightly smaller, but they remain near the ballistic regime.

For disordered chains, we observe drastic changes in γ as we increase F_0. Specifically, the mean values of the exponents for the disordered chains diminish gradually from superdiffusive ones ($1 < \gamma < 2$) to subdiffusive ones ($0 < \gamma < 1$) for chains with progressively stronger static precompressions. This is more noticeable in our numerical simulations than in our experimental data; in the latter, we clearly observe the superdiffusive regime, yet our measurements while approaching the diffusive regime do not definitively manifest subdiffusive behavior. In simulations, in contrast, our ability to do a large variety of numerical experiments allows us to collect data for numerous precompression strengths and to transparently reveal the trend from superdiffusion to subdiffusion. It is also important to contrast our subdiffusive numerical results, for which we observe $\gamma \in (0.5,1)$, with the much slower subdiffusive spreading in discrete nonlinear Schrödinger and Klein–Gordon chains[6–8]. Our experimental results (white squares) indicate that the exponent γ of the second moment of the kinetic energy is smaller for progressively stronger

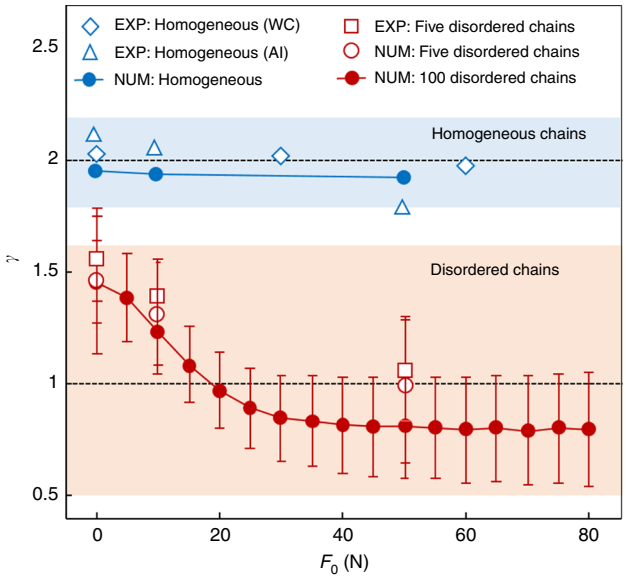

Fig. 5 Energy-spreading characteristics. Exponents (γ) of the second moment m_2 of kinetic energy as a function of precompression strength. The exponents 1 and 2 (horizontal dashed lines) represent diffusive and ballistic transport, respectively. The diamond, triangular, and square marks are based on experimental data obtained, respectively, from a homogeneous tungsten-carbide (WC) chain, a homogeneous aluminum (Al) chain, and a mean over five disordered chains. (See Supplementary Table 1 and Supplementary Note 1 for details about the five disordered chains.) We mark the numerical data with circles. We do computations for homogeneous chains (blue circles), the five disordered chains (hollow red circles), and 100 randomly generated disordered chains (red circles with error bars). The red circles and error bars, respectively, give the mean values and standard deviations of the computed exponents from the 100 cases

precompression F_0, in line with our numerical observations (white circles). However, while our experimental findings definitively manifest superdiffusion, they are inconclusive about the potential transition to subdiffusion as one increases F_0.

We also compare the exponents that we obtain from the five disordered chains with those from numerical simulations of 100 different disordered chains in Fig. 5. The red circles and error bars, respectively, give the mean values and standard deviations of the computed exponents from the 100 cases. The relevant trends persist despite the larger error bars for stronger precompressions. The agreement between computations and experiments also continues to hold. Additionally, although our study focuses on

the effect of nonlinearity and disorder, the boundary conditions in granular chains can also alter energy transport mechanisms, as demonstrated previously in other physical systems (e.g., refs. [27,28]). See Supplementary Fig. 5 and Supplementary Note 6 for detailed numerical calculations of such boundary effects.

Discussion

In this study, we experimentally and numerically investigate energy transport and localization properties in both ordered and disordered one-dimensional granular crystals in strongly nonlinear, weakly nonlinear, and almost linear settings. In our experiments, we observe exponential attenuation of the energy distribution for disordered chains when we apply strong precompression to obtain almost linear dynamics. This is reminiscent of Anderson localization. We show that this localized pattern oscillates persistently near the chain boundary. For progressively weaker precompression, the system's effective nonlinearity becomes stronger, and there is a gradual progression from a localized pattern to flatter energy distributions. This affects the chain's transport properties, as energy spreads faster for weaker precompression.

Our study paves the way toward using granular crystals and related systems (e.g., ones involving magnets[29]) as accessible platforms for exploring the interplay between nonlinearity and disorder in a lattice setting. The amenability of such granular metamaterials for controllable tuning between strongly nonlinear and almost linear regimes, coupled with the ability to monitor such systems in a distributed fashion, promises a wealth of exciting advances in condensed-matter physics, materials science, and nonlinear dynamics. Proposals to engineer local nonlinearity effects (e.g., see ref. [30]) in granular crystals and to examine the competition between the chiefly superdiffusive effects of inter-site nonlinearities and the apparently chiefly subdiffusive effects of on-site nonlinearities also constitute important future directions.

Methods

Experiments. We measure wave propagation in two types of one-dimensional granular crystals (i.e., granular chains): homogeneous and disordered chains. Each chain consists of 32 particles using either tungsten-carbide (Young modulus $E = 600$ GPa, Poisson ratio $\nu = 0.2$, and density $\rho = 15.6$ g cm^{-3}) or aluminum ($E = 69$ GPa, $\nu = 0.33$, and $\rho = 2.8$ g cm^{-3}). The radius of each particle is 9.53 mm. The values of E, ν, and ρ are based on standard specifications[31]. We examine two homogeneous chains (one made of tungsten-carbide and the other made of aluminum) and five disordered chains (with combinations of tungsten-carbide and aluminum, as described in Supplementary Table 1 and Supplementary Note 1). In the disordered chains, we randomly choose each particle, except for the first particle, as either a tungsten-carbide or aluminum particle, with an independent 50% probability of each for each particle. This yields an 'uncorrelated' type of disorder[11]. As we illustrate in Supplementary Fig. 6 and Supplementary Note 7, a 32-particle granular chain is long enough to validate energy localization and transport properties.

The spherical particles are supported by two stainless-steel rods coated by polytetrafluoroethylene (PTFE) tape to reduce friction between the particles and the supporting rods. We also place two aluminum rods on top of the granular chain, with minimum clearance to restrict lateral motion of the particles. To apply various precompression strengths to a chain, we press a heavy block on a sliding guide toward the chain using a linear spring. Between the block and the chain, we embed a static force sensor (see Fig. 1) to ensure accurate monitoring of the precompression applied to the chains. The other side of a chain is blocked by a steel plate with a circular hole in the center, and we bond four equidistant steel balls to the edge of the hole (see the inset of Fig. 1). These balls have point contacts with the first particle; this yields a much smaller contact damping between the first particle and the plate boundary than one would obtain from a line contact between the two.

For this study, we test granular chains with various precompression strengths (from 0 to 60 N). We give an impact excitation to the first particle using a chrome-steel ($E = 210$ GPa, $\nu = 0.29$, and $\rho = 7.8$ g cm^{-3}) particle with a 4.75 mm radius. We roll the particle down a ramp so that it has a normal impact on the first particle through the hole of the plate (see Fig. 1). The impact velocity, which we measure using a laser Doppler vibrometer (Polytec OFV 534), is 0.45 ± 0.12 m s^{-1}.

To visualize wave propagation in a granular chain, we measure the axial velocities of particles individually for each particle spot using the LDV. To synchronize the measured data, we use a small piezoelectric ceramic plate (3 mm × 4 mm × 0.5 mm) bonded to the first particle; this plate generates a trigger signal (voltage) at the instant of striker impact. We scan the velocity profiles for all particles in the chain by moving the LDV using a moving stage, and we reconstruct the measured data to depict a spatiotemporal profile of propagating waves. For each configuration, we follow the above procedures and conduct three tests. This amounts to 672 experimental realizations to construct the spatiotemporal dynamics of the granular chains for all of the cases that we study in the present article.

Numerical simulations. The equation of motion for the i^{th} particle in a granular chain is[16]

$$m_i \frac{\mathrm{d}^2 u_i}{\mathrm{d}t^2} = A_{i-1,i}\left[\delta_{i-1,i} + u_{i-1} - u_i\right]_+^{3/2} - A_{i,i+1}\left[\delta_{i,i+1} + u_i - u_{i+1}\right]_+^{3/2} - \frac{m_i}{\tau}\frac{\mathrm{d}u_i}{\mathrm{d}t}, \quad (3)$$

where m_i and u_i, respectively, are the mass and displacement of the i^{th} particle. The force on the i^{th} particle depends on the geometry and material properties of both it and its adjacent particles. The interaction coefficient between the i^{th} and $(i+1)^{\text{th}}$ particles is

$$A_{i,i+1} = \frac{4E_iE_{i+1}}{3\left[E_{i+1}(1-\nu_i^2) + E_i(1-\nu_{i+1}^2)\right]}\sqrt{\frac{R_iR_{i+1}}{R_i + R_{i+1}}}, \quad (4)$$

where E_i, ν_i, and R_i are, respectively, the i^{th} particle's Young modulus, Poisson ratio, and radius. The quantity $\delta_{i,i+1} = (F_0/A_{i,i+1})^{2/3}$ is the compression distance between the i^{th} and $(i+1)^{\text{th}}$ particles at static equilibrium under a static precompression of F_0. The bracket $[x]_+ = \max\{0,x\}$ encodes the fact that there are no tensile forces in interparticle interactions. We determine the damping coefficient $1/\tau$ by measuring the decay of leading waves in experiments and calculating a value for τ that matches the experimental results. (See Supplementary Fig. 7 and Supplementary Note 8 for further discussion about the effect of dissipation on energy spreading. See Supplementary Note 9 for a brief discussion about testing for plasticity.) For the homogeneous chain of aluminum particles, we use $\tau = 2$ ms (for $F_0 = 0$ N), $\tau = 1$ ms (for $F_0 = 10$ N), and $\tau = 0.4$ ms (for $F_0 = 50$ N). For the disordered chains, we use $\tau = 1$ ms (for $F_0 = 0$ N), $\tau = 0.6$ ms (for $F_0 = 10$ N), and $\tau = 0.4$ ms (for $F_0 = 50$ N).

The equation of motion for the striker particle ($i = 0$) includes an interparticle interaction only with the first particle, and the first particle interacts with the boundary plate and the second particle (in addition to the striker). Similarly, the last particle has an interaction with the penultimate particle and the other boundary plate. The displacements at the boundaries are fixed ($u_{\text{left}} = u_{\text{right}} = 0$), and we apply an initial velocity to the striker ($v_{\text{striker}} = 0.45$ m s^{-1}). We conduct numerical simulations using a variety of different impact velocities of about 0.45 m s^{-1} and observe no significant differences in the exponents. More generally, the presence of both superdiffusive transport and wave localization, which we see in the values of both m_2 and P^{-1}, is robust to changes in the initial condition of the impactor.

We solve the equations of motion (3) numerically with a Runge–Kutta method (of Dormand–Prince type) using Matlab's ODE45 routine with a relative error tolerance of 0.1%. In calculations with lower error tolerances, we obtain the same results. Based on the relative tolerance of 0.1%, the order of magnitude of the error in the displacements is less than 1×10^{-9} m, and the order of magnitude of the error in the velocities is less than an amount ranging from 1×10^{-6} to 1×10^{-4} m s^{-1}, depending on the specific properties of the waves.

Using numerical simulations, we probe additional details of disordered granular chains. In addition to those that we discussed earlier, we compare the dynamics in velocity excitations and displacement excitations (see Supplementary Fig. 6 and Supplementary Note 10). We also consider a sub-ensemble in which the first particle is tungsten-carbide. In this case, in contrast to the sub-ensemble in which the first particle is aluminum (for which localization occurs around the second particle), we observe that localization tends to occur around the first particle (see Supplementary Fig. 8 and Supplementary Note 11).

Data availability. The data sets generated and analyzed during the current study are available from the corresponding author on reasonable request.

Received: 1 June 2017 Accepted: 11 January 2018
Published online: 13 February 2018

References

1. Anderson, P. W. Absence of diffusion in certain random lattices. *Phys. Rev.* **109**, 1492 (1958).
2. Lagendijk, A., van Tiggelen, B. & Wiersma, D. S. Fifty years of Anderson localization. *Phys. Today* **62**(8), 24 (2009).
3. Roati, G. et al. Anderson localization of a non-interacting Bose–Einstein condensate. *Nature* **453**, 895–898 (2008).

4. Billy, J. et al. Direct observation of Anderson localization of matter waves in a controlled disorder. *Nature* **453**, 891–894 (2008).
5. Segev, M., Silberberg, Y. & Christodoulides, D. N. Anderson localization of light. *Nat. Photon.* **7**, 197–204 (2013).
6. Flach, S. in *Nonlinear Optical and Atomic Systems, Lecture Notes in Mathematics* Vol. 2146 (eds Besse, C. & Garreau, J. C.) Ch. 1 (Switzerland, Springer, 2015).
7. Kopidakis, G., Komineas, S., Flach, S. & Aubry, S. Absence of wave packet diffusion in disordered nonlinear systems. *Phys. Rev. Lett.* **100**, 084103 (2008).
8. Flach, S., Krimer, D. O. & Skokos, Ch. Universal spreading of wave packets in disordered nonlinear systems. *Phys. Rev. Lett.* **102**, 024101 (2009).
9. Campbell, D. K., Rosenau, P. & Zaslavsky, G. M. Introduction: The Fermi–Pasta–Ulam problem—The first fifty years. *Chaos* **15**, 015101 (2005).
10. Galavotti, G. (Ed.) *The Fermi–Pasta–Ulam Problem: A Status Report* (Springer-Verlag, NY, 2008).
11. Martínez, A. J., Kevrekidis, P. G. & Porter, M. A. Superdiffusive transport and energy localization in disordered granular crystals. *Phys. Rev. E* **93**, 022902 (2016).
12. Achilleos, V., Theocharis, G. & Skokos, Ch. Energy transport in one-dimensional disordered granular solids. *Phys. Rev. E* **93**, 022903 (2016).
13. Mulansky, M. & Pikovsky, A. Energy spreading in strongly nonlinear disordered lattices. *N. J. Phys.* **15**, 053015 (2013).
14. Flach, S. & Gorbach, A. Discrete breathers: Advances in theory and applications. *Phys. Rep.* **467**, 1–116 (2007).
15. Nesterenko, V. F. *Dynamics of Heterogeneous Materials* (Springer, New York, 2001).
16. Sen, S., Hong, J., Bang, J., Avalos, E. & Doney, R. Solitary waves in the granular chain. *Phys. Rep.* **462**, 21–66 (2008).
17. Porter, M. A., Kevrekidis, P. G. & Daraio, C. Granular crystals: Nonlinear dynamics meets materials engineering. *Phys. Today* **68**(11), 44–50 (2015).
18. Chong, C., Porter, M. A., Kevrekidis, P. G. & Daraio, C. Nonlinear coherent structures in granular crystals. *J. Phys. Condens. Matter* **29**, 413003 (2017).
19. Johnson, K. L. *Contact Mechanics* (Cambridge University Press, Cambridge, 1985).
20. Nguyen, N. S. & Brogliato, B. *Multiple Impacts in Dissipative Granular Chains* (Springer-Verlag, Berlin, 2014).
21. Achilleos, V., Theocharis, G. & Skokos, Ch. Polydispersed granular chains: From long-lived chaotic Anderson-like localization to energy equipartition. Preprint at https://arxiv.org/abs/1707.03162 (2017).
22. Kim, E. et al. Nonlinear low-to-high frequency energy cascades in diatomic granular crystals. *Phys. Rev. E* **92**, 062201 (2015).
23. Daraio, C., Nesterenko, V. F., Herbold, E. B. & Jin, S. Tunability of solitary wave properties in one-dimensional strongly nonlinear phononic crystals. *Phys. Rev. E* **73**, 026610 (2006).
24. Laptyeva, T. V., Ivanchenko, M. V. & Flach, S. Nonlinear lattice waves in heterogeneous media. *J. Phys. A* **47**, 493001 (2014).
25. English, J. M. & Pego, R. L. On the solitary wave pulse in a chain of beads. *Proc. Am. Math. Soc.* **133**, 1763–1768 (2005).
26. Datta, P. K. & Kundu, K. Energy transport in one-dimensional harmonic chains. *Phys. Rev. B* **51**, 6287–6295 (1995).
27. Szameit, A. et al. Wave localization at the boundary of disordered photonic lattices. *Opt. Lett.* **35**, 1172 (2010).
28. Molina, M. I., Lazarides, N. & Tsironis, G. P. Optical surface modes in the presence of nonlinearity and disorder. *Phys. Rev. E* **85**, 017601 (2012).
29. Molerón, M., Leonard, A. & Daraio, C. Solitary waves in a chain of repelling magnets. *J. Appl. Phys.* **115**, 184901 (2014).
30. James, G., Kevrekidis, P. G. & Cuevas, J. Breathers in oscillator chains with Hertzian interactions. *Phys. D* **251**, 39 (2013).
31. ASM International. *ASM International Metals Handbook* (ADM International, 1990).

Acknowledgements

A.J.M. acknowledges support from CONICYT (BCH72130485/2013). J.Y. thanks the NSF (CAREER-1553202) for financial support. J.Y. and P.G.K. also acknowledge support from US-ARO (W911NF-15-1-0604) and US-AFOSR (FA9550-17-1-0114), and P.G.K. also gratefully acknowledges support from the Stavros Niarchos Foundation via the Greek Diaspora Fellowship Program. E.K. acknowledges the support from the National Research Foundation of Korea (NRF) grant funded by the Korea government (MSIP, No. 2017R1C1B5018136)

Author contributions

All authors wrote the paper and contributed equally to the production of the manuscript and interpretation of results; P.G.K., A.J.M., M.A.P., and J.Y. designed the study; E.K. and S.E.P. performed the experiments; and E.K., A.J.M., and S.E.P. did the numerical computations and data analysis.

Additional information

Supplementary Information accompanies this paper at https://doi.org/10.1038/s41467-018-03015-3.

Competing interests: The authors declare no competing financial interests.

Reprints and permission information is available online at http://npg.nature.com/reprintsandpermissions/

Publisher's note: Springer Nature remains neutral with regard to jurisdictional claims in published maps and institutional affiliations.

SUPPLEMENTARY FIGURES

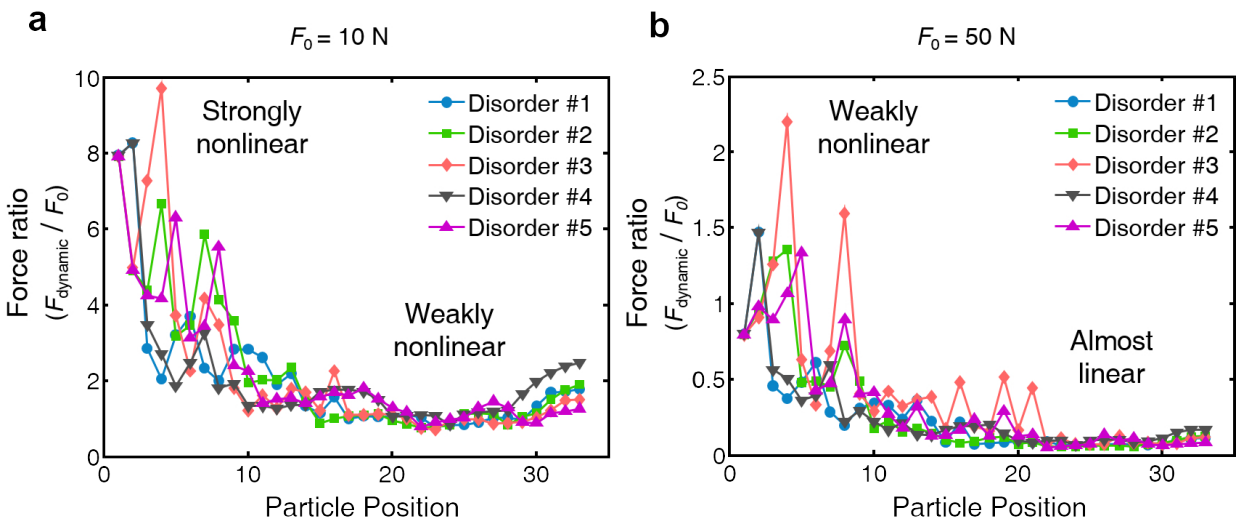

Supplementary Figure 1. **Ratio of maximum dynamic force to static precompression.** (**a**) Ratio of the maximum dynamic force (defined as $F_{\text{dynamic}} = \max(|F - F_0|)$, where F is the propagating wave's force amplitude) to the static precompression F_0 in disordered chains for $F_0 =$ 10 N . (**b**) Ratio of maximum dynamic force to the static precompression in disordered chains for $F_0 = 50$ N.

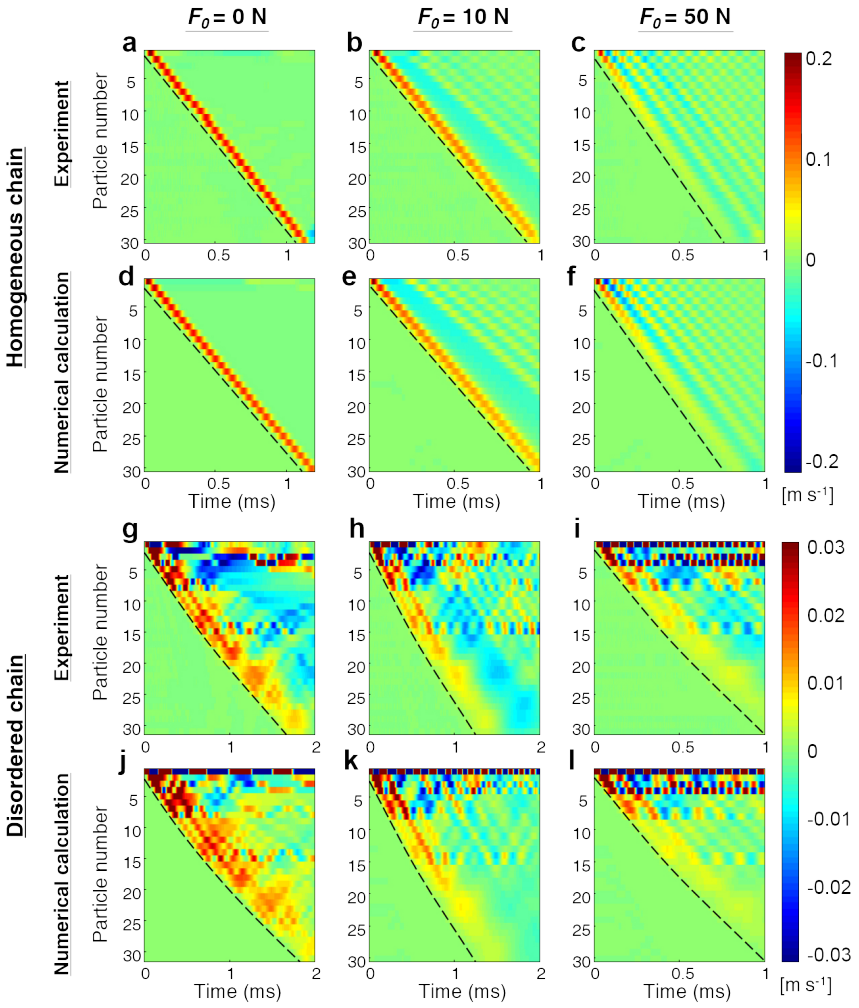

Supplementary Figure 2. **Wave propagation in homogeneous and disordered chains.** (**a**–**f**) Spatiotemporal distributions of particle velocities in a homogeneous chain consisting of aluminum particles with static precompressions of (**a**,**d**) 0 N, (**b**,**e**) 10 N, and (c,f) 50 N. We compare the experimental data (panels **a**–**c**) to numerical simulations (panels **d**–**f**). (**g**–**l**) Spatiotemporal distributions of particle velocities in a disordered chain (the 'Chain 1' configuration in Supplementary Table I) with static precompressions of (**g**,**j**) 0 N, (**h**,**k**) 10 N, and (**i**,**l**) 50 N. We compare the experimental data (panels **g**–**i**) to numerical calculations (panels **j**–**l**). We show dashed arcs to visually track the edges of the velocity distributions.

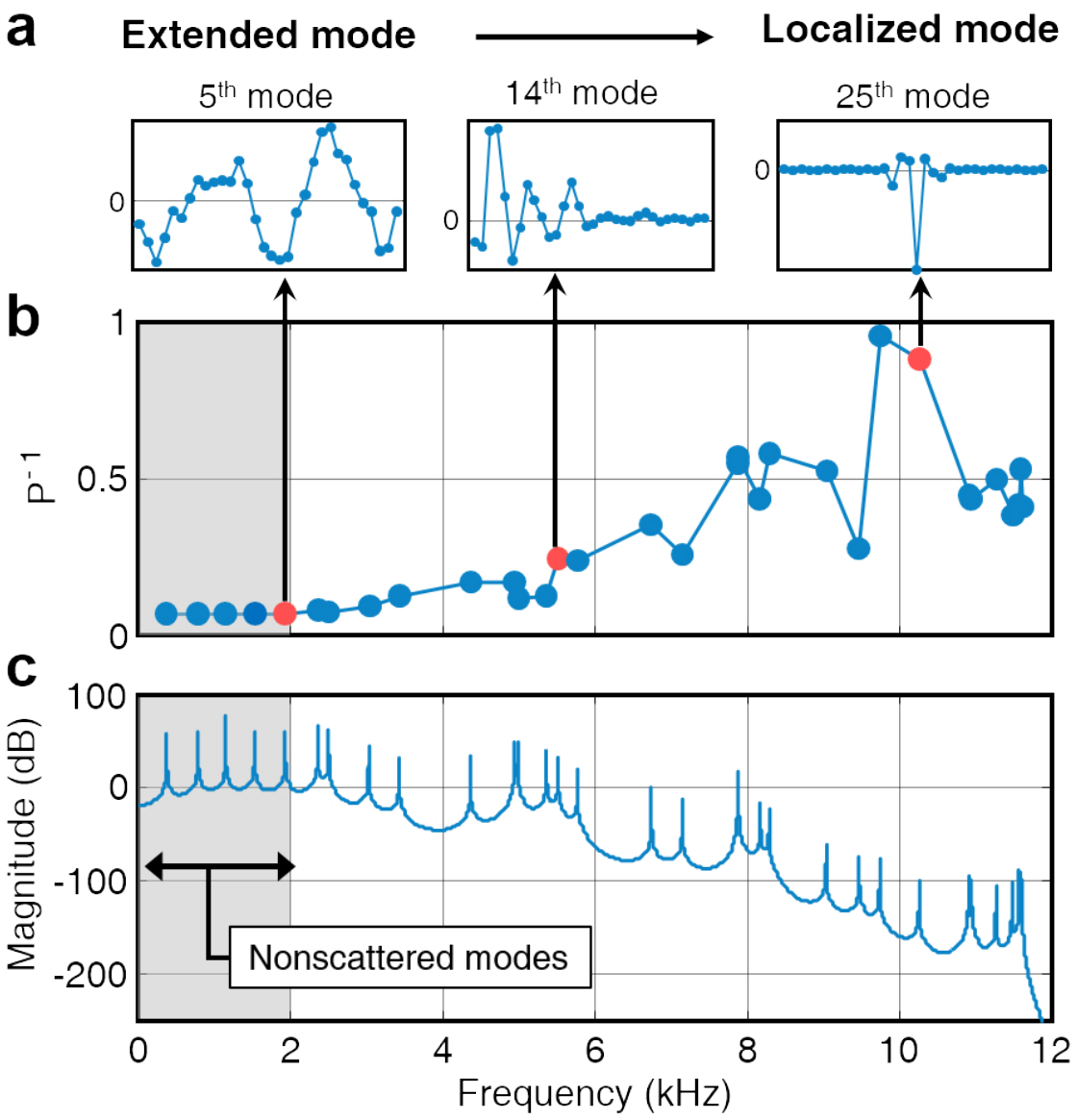

Supplementary Figure 3. **Vibration modes of a disordered chain (Chain 1 from Supplementary Table I) for a static precompression of $F_0 = 50$ N.** (**a**) Mode profiles of the 5$^{\text{th}}$, 14$^{\text{th}}$, and 25$^{\text{th}}$ modes. (**b**) Inverse participation ratio (IPR) P^{-1} calculated based on the displacement amplitude for each mode. (**c**) Frequency response function of the disordered chain. The shaded area shows the nonscattered modes (from the 1$^{\text{st}}$ to the 5$^{\text{th}}$ modes).

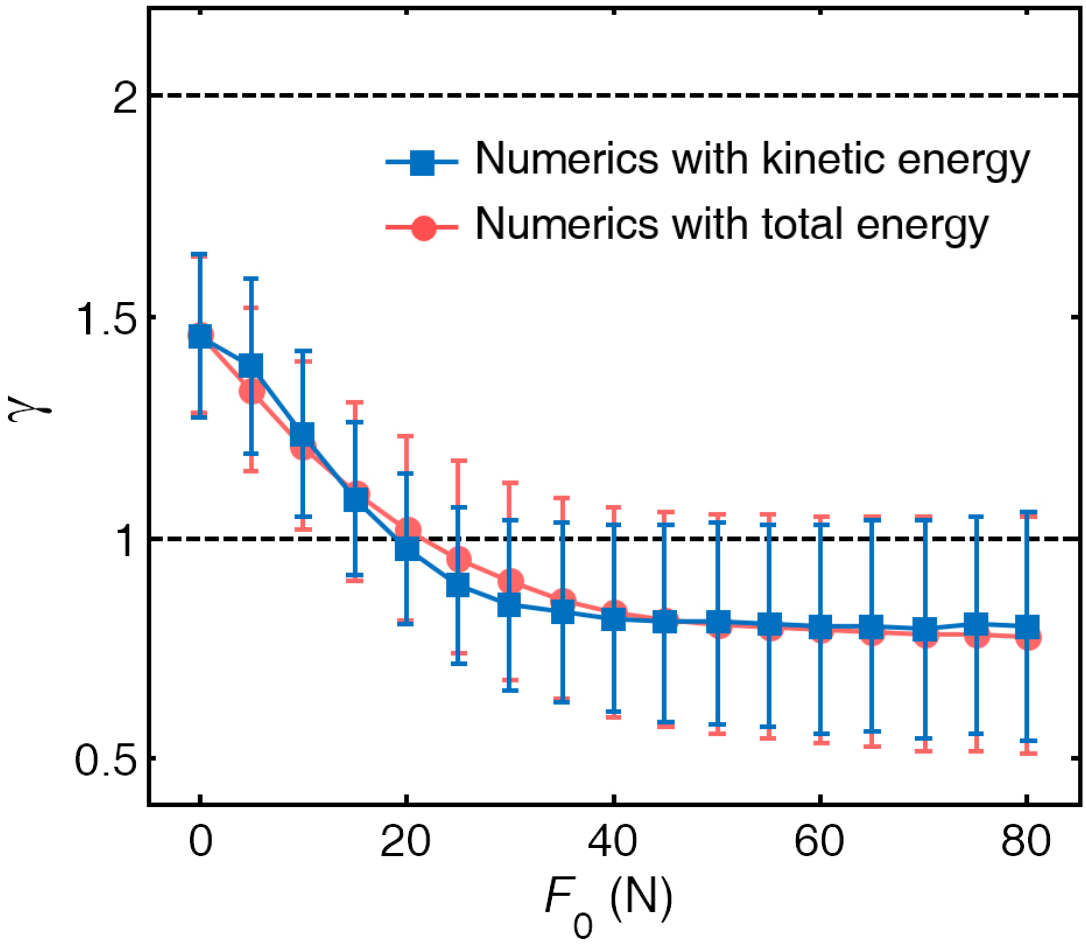

Supplementary Figure 4. **Comparison of second moments from kinetic energy versus those from total energy for different precompression strengths in our numerical simulations of disordered chains.** The blue squares represent calculations based on kinetic energy, and the red circles represent calculations based on total energy (i.e., kinetic energy plus potential energy). The vertical axis gives the exponent γ of the second moment, and the horizontal axis gives the static precompression strength. For these simulations, we use 32-particle chains and a velocity excitation.

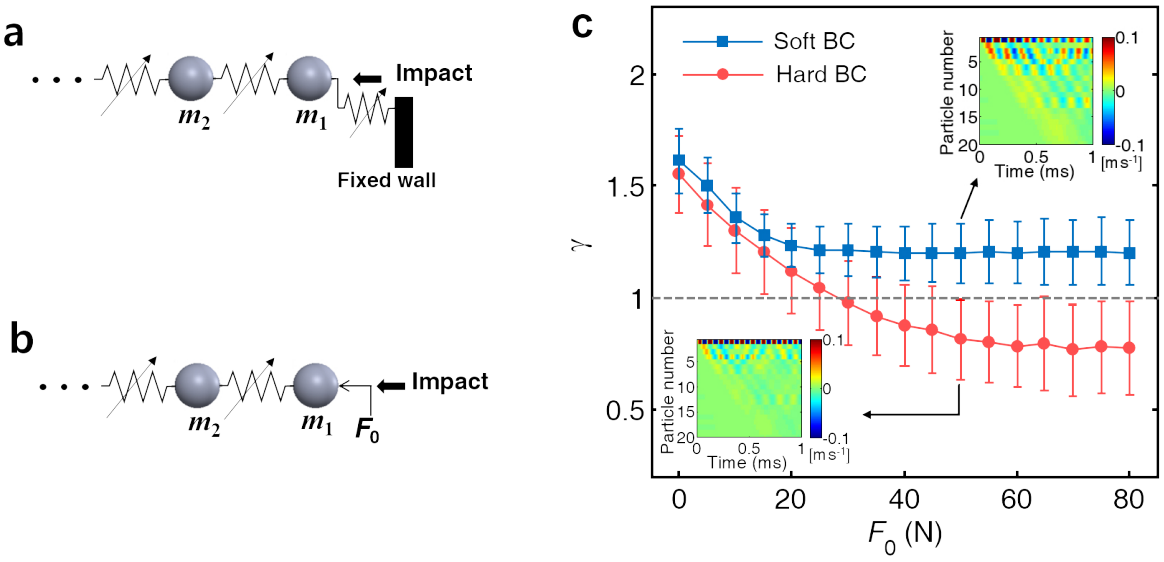

Supplementary Figure 5. **Boundary conditions at the location of the excitation and their corresponding effects on energy transport.** (**a**) Schematic of an excitation as a hard boundary constrained by a fixed wall. (**b**) Schematic of an excitation as a soft boundary (specifically, a free boundary) in which precompression is applied directly to the first particle without any constraints. In both panels, the depicted springs represent Hertzian interactions. (**c**) Comparison of the second moment m_2 of the kinetic energy, averaged over 100 realizations, for granular chains with two different boundary conditions at the right end: a hard boundary (red circles) and soft boundary (blue squares). The insets represent spatiotemporal distributions of the propagation velocity for particles in chains with the two different boundary conditions.

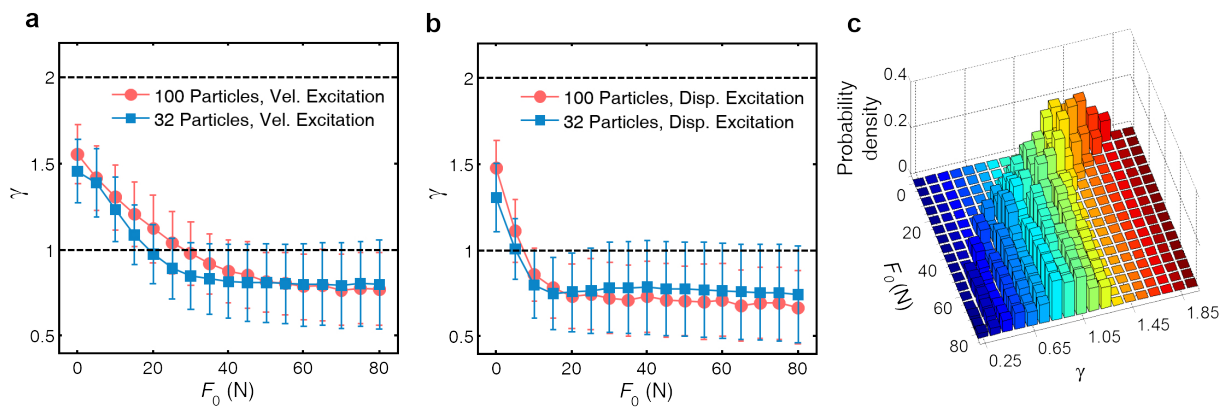

Supplementary Figure 6. **Comparison of exponents γ of the second moment m_2 of the kinetic energy in short versus long chains.** We compare the exponents between short chains (32 particles) and long chains (100 particles) for (**a**) a velocity excitation and (**b**) a displacement excitation. We use 100 chains for each case, and we generate them randomly by independently choosing each particle in the chain as either tungsten-carbide and aluminum particles with equal probability. (**c**) Probability density as a function of statistic precompression F_0 and spreading exponent γ.

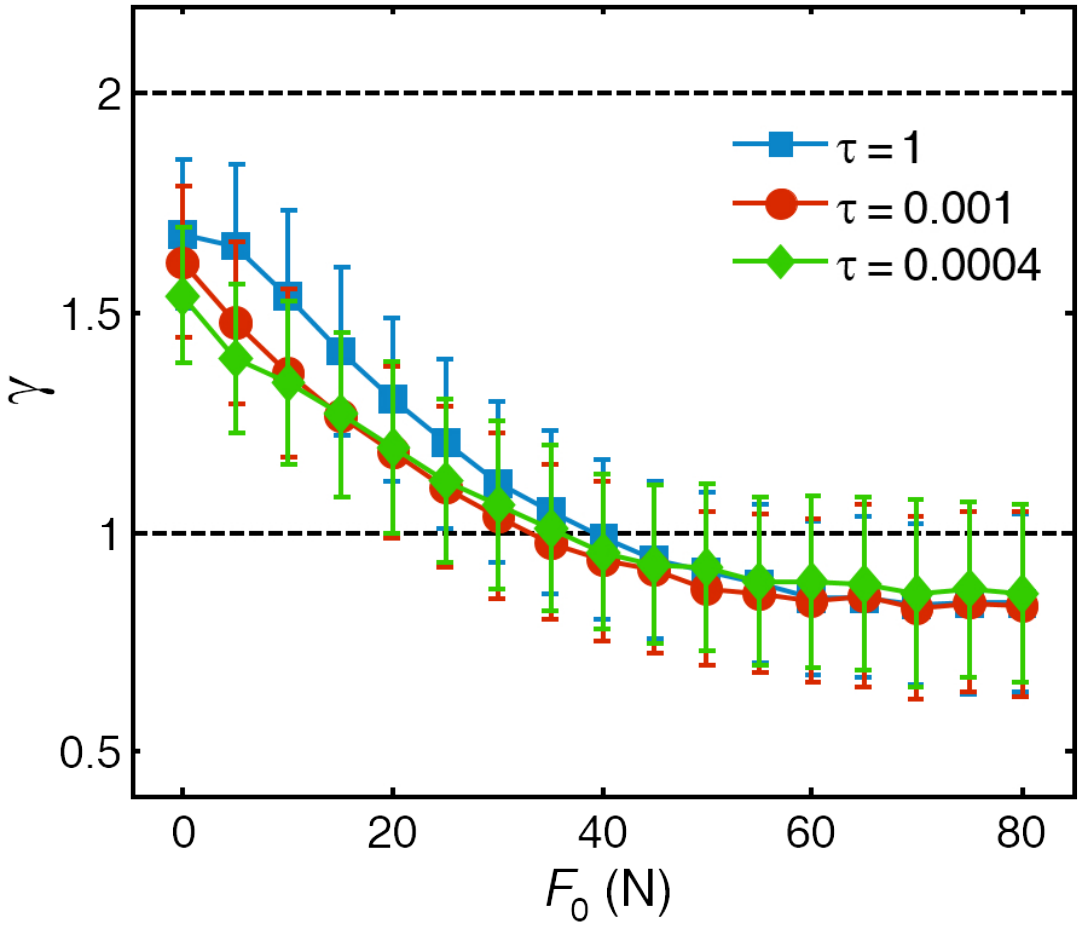

Supplementary Figure 7. **Effect of dissipation on energy spreading in disordered chains.** Exponent γ of the second moment m_2 of kinetic energy for various dissipation coefficients $(1/\tau)$ as a function of precompression strength. We show means of numerical simulations from 100 disordered chains with 100 particles each over the time period $[0.1, 3]$ ms.

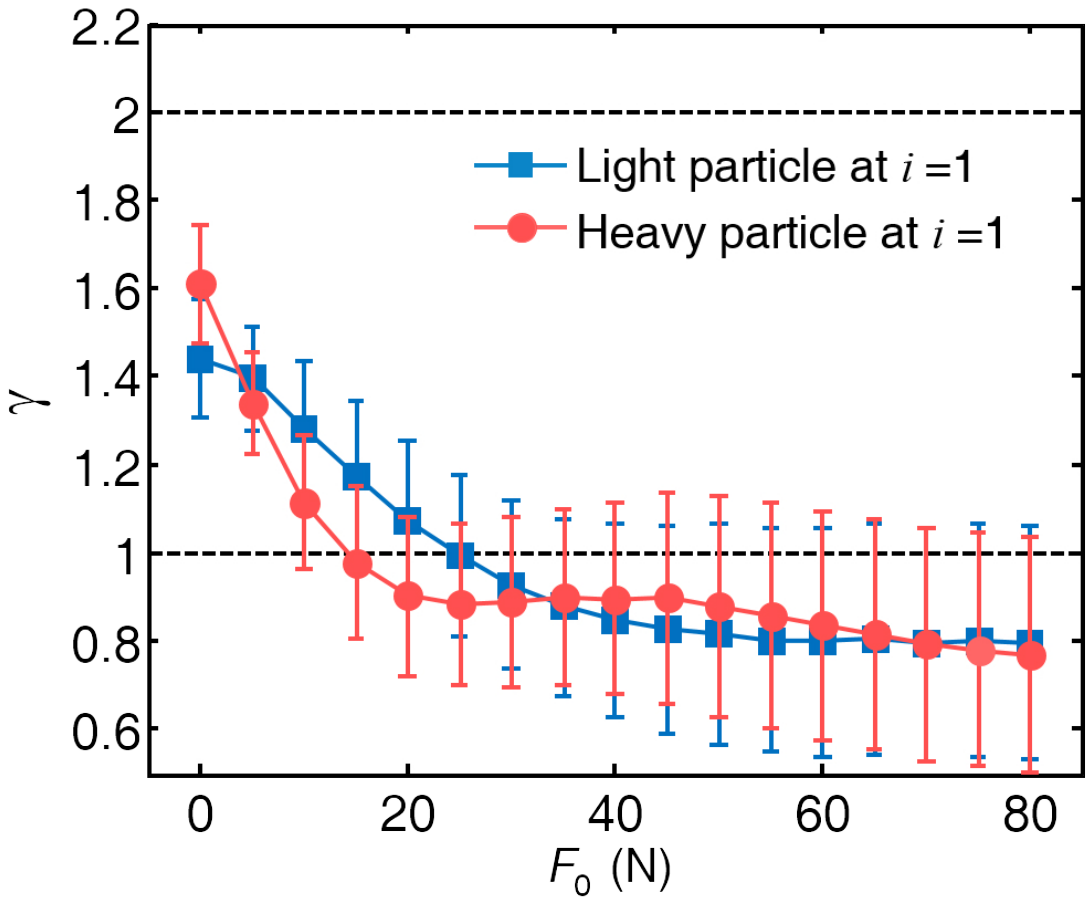

Supplementary Figure 8. **Effect of the choice of material of the first particle on energy spreading.** We compare the exponent γ of the second moment m_2 of the kinetic energy between chains that have a light particle (aluminum) at $i = 1$ (i.e., in the first position) and chains that have a heavy particle (tungsten-carbide) at $i = 1$. All chains have 100 particles and a fixed-wall boundary at the right.

SUPPLEMENTARY TABLE

Supplementary Table I. Configurations of the five disordered chains in our experiments.

Disordered chain	Order of particles (1: Tungsten-Carbide; 2: Aluminum)
Chain 1	[2, 1, 2, 2, 1, 1, 2, 2, 1, 1, 1, 1, 1, 2, 2, 1, 2, 1, 2, 2, 1, 1, 2, 2, 2, 1, 2, 1, 1, 1, 2, 1]
Chain 2	[2, 2, 2, 1, 2, 1, 1, 1, 1, 2, 1, 2, 1, 1, 2, 2, 2, 1, 1, 2, 1, 2, 2, 1, 2, 2, 1, 1, 2, 1, 1, 1]
Chain 3	[2, 2, 1, 1, 2, 2, 1, 1, 2, 2, 2, 2, 2, 2, 2, 1, 2, 1, 1, 1, 1, 2, 1, 2, 2, 1, 1, 2, 1, 1, 1, 2]
Chain 4	[2, 1, 2, 2, 2, 2, 1, 2, 1, 2, 2, 1, 2, 1, 2, 1, 1, 1, 1, 1, 2, 2, 1, 1, 2, 2, 1, 1, 1, 1, 1, 1]
Chain 5	[2, 2, 2, 2, 1, 2, 1, 1, 2, 1, 2, 2, 1, 2, 2, 1, 1, 1, 1, 2, 1, 2, 2, 2, 1, 1, 1, 1, 2, 1, 2, 1]

SUPPLEMENTARY NOTE 1: NUMERICAL AND EXPERIMENTAL RESULTS FROM HOMOGENEOUS AND DISORDERED GRANULAR CHAINS, AND THE DETAILED CONFIGURATIONS OF THE DISORDERED CHAINS.

In Supplementary Figure 2, we show the full-field particle velocities for a homogeneous chain that consists of aluminum particles only (top two rows) and a disordered chain composed of aluminum and tungsten-carbide particles (bottom two rows) in strongly nonlinear, weakly nonlinear, and almost linear scenarios (in the left, middle, and right panels, respectively). In each group, the upper and lower rows show our experimental and numerical results, respectively. Our numerical results corroborate our experimental measurements.

In Supplementary Figure 2 and also in Figure 2 of the main manuscript, we report disordered-chain results for the first configuration ('Chain 1') of the 32-particle disordered chains from Supplementary Table I. We assemble each disordered chain by randomly choosing each individual particle (except for the first one) in the chain as either aluminum or tungsten-carbide with equal probability. This splits the statistical ensemble into two sub-ensembles: (i) chains with the first particle fixed as aluminum and (ii) chains with the first particle fixed as tungsten-carbide. We intentionally choose to examine case (i), because it facilitates transfer of mechanical energy from the striker particle to the chain. This observation is based on preliminary experimental observations using both sub-ensembles. In this case, our experiments have mean energy transfer rates from the striker to the chain of 75.5%, 76.1%, and 85.8% for 0 N, 10 N, and 50 N precompression, respectively. Although we focus our experimental efforts on studying case (i), we show numerically that case (ii) has similar transport properties as case (i). For instance, in both cases, we observe a transition from subdiffusive to superdiffusive behavior, although the precise values for the energy spreading-rate exponents γ differ. (See Supplementary Note 11 for more details.)

SUPPLEMENTARY NOTE 2: NONLINEARITY OF STRESS WAVES PROPAGATING IN DISORDERED CHAINS.

In a disordered granular chain, stress waves scatter as they propagate along the chain, which in turn results in a diminution of the wave amplitude. When one applies precom-

pression to a chain, this amplitude decrease changes the nonlinearity strength in the system as the stress waves propagate along the chain. One can estimate the nonlinearity strength of the propagating wave based on the ratio of its dynamic force to the static precompression. We use the following qualitative criterion for characterizing regimes with different nonlinearity strengths. We say that dynamics is 'strongly nonlinear' when the force ratio $F_{\text{dynamic}}/F_0 \gg 1$, 'weakly nonlinear' when $F_{\text{dynamic}}/F_0 \approx 1$, and 'almost linear' (which is also known as 'nearly linear', or sometimes just 'linear' as a shorthand) when $F_{\text{dynamic}}/F_0 \ll 1$. The maximum dynamic force is $F_{\text{dynamic}} = \max(|F - F_0|)$, where F is the propagating wave's force amplitude and F_0 is the static precompression. In Supplementary Figure 1a, we show F_{dynamic}/F_0 when $F_0 = 10$ N. Initially, a strongly nonlinear wave forms, but it subsequently becomes a weakly nonlinear one due to scattering and localization. In Supplementary Figure 1b, we show the force ratio for $F_0 = 50$ N precompression, where a weakly nonlinear wave becomes an almost linear one as it propagates.

SUPPLEMENTARY NOTE 3: LINEAR MODES OF A DISORDERED CHAIN AND ITS FREQUENCY RESPONSE FUNCTION.

When precompression is strong enough compared to the dynamic force, one can linearize Equation (3) in the main text. Using this linearization, one obtains an approximate description of a granular chain's dynamics as a superposition of the temporal evolution of different vibration modes. The weight of each mode depends on the initial excitation. For a disordered chain, vibration modes with predominantly low frequencies are delocalized, producing what are sometimes called 'nonscattered modes'[1]. The number q_{ns} of nonscattered modes satisfies $q_{\text{ns}} \sim \sqrt{N}$ as $N \to \infty$, where N is the total number of particles in the chain. In our 32-particle chains, roughly the first six modes are nonscattered modes. Consequently, the waves with frequencies associated with nonscattered modes tend to propagate along the chain without localization. For progressively higher frequencies, vibration modes become localized, reducing the effective number of particles that oscillate with an amplitude that differs substantially from 0. We quantify this phenomenon by computing the inverse participation ratio (IPR) P^{-1}, which we show in Supplementary Figure 3. We also show representative vibration modes and frequency response functions of a disordered chain (using Chain 1 from Supplementary Table I) at $F_0 = 50$ N. Because the IPR represents the degree

of localization, an extended mode — corresponding to a low-frequency wave mode with a long wavelength — has a low value of P^{-1}, whereas a localized mode has P^{-1} close to 1.

SUPPLEMENTARY NOTE 4: EXPONENTIAL FIT OF KINETIC-ENERGY DECAY IN THE ANDERSON-LIKE MODE.

To support the exponential fit that we use to characterize the early decay of the kinetic-energy distribution (see Figure 3 in the main manuscript), we perform an Anderson–Darling test[2]. Because we estimate the parameter of the exponential trend from data, to implement the test, we apply a Monte-Carlo procedure with 1000 data sets generated under the null hypothesis of the exponential distribution $\bar{K}_i \propto e^{-0.54i}$. Using particles $i \in \{2, \ldots, 10\}$, we obtain a p-value of 0.96, so it passes the standard statistical test indicating that there is no significant departure from normality.

SUPPLEMENTARY NOTE 5: COMPARISON OF SPREADING EXPONENT γ BETWEEN KINETIC ENERGY AND TOTAL ENERGY.

In Supplementary Figure 4, we compare the exponents γ of the second moment ($m_2(t) \sim t^{\gamma}$) of the kinetic energy with those that we calculate using the total energy in our numerical simulations of 32-particle disordered chains with a velocity excitation (see Supplementary Note 10). This figure illustrates that, despite the observed oscillations of $m_2(t)$ because of the kinetic–potential energy exchange in the propagating waves, the exponents of the experimentally measurable kinetic energy are essentially the same as those obtained from total energy.

SUPPLEMENTARY NOTE 6: BOUNDARY EFFECTS

Previous studies reported that when the disorder is uncorrelated (as in our case), velocity excitations in the bulk exhibit superdiffusive transport regardless of the nonlinear regime, whereas displacement excitations transition from subdiffusive transport in the almost linear regime to superdiffusive spreading in the strongly nonlinear regime[3,4]. Interestingly, when we excite the first particle at the fixed boundary of a granular chain, we observe that both velocity and displacement excitations have a transition from subdiffusive to superdiffusive

transport (see Supplementary Figure 6). To investigate the effect of boundary conditions on energy-transport mechanisms, we conduct numerical simulations using 100-particle chains and compare two scenarios. One scenario is a hard boundary fixed with a massive wall (as in the experimental setup), and the other is a soft boundary in which we apply a consistent precompression force to the first particle (see Supplementary Figures 5a,b). For a fixed boundary with a wall, the boundary particle ($i = 1$) interacts with three objects: the striker ($i = 0$), an adjacent particle ($i = 2$), and the wall ($i = w$). Its equation of motion is

$$\begin{aligned} m_1 \frac{d^2 u_1}{dt^2} = & A_{0,1} \left[\delta_{0,1} + u_0 - u_1\right]_+^{3/2} - A_{1,2} \left[\delta_{1,2} + u_1 - u_2\right]_+^{3/2} \\ & + A_{w,1} \left[\delta_{w,1} - u_1\right]_+^{3/2} - \frac{m_1}{\tau} \frac{du_1}{dt} \,, \end{aligned} \tag{1}$$

where first and second terms on the right-hand side represent, respectively, the interactions of the first particle with the striker and the second particle. The third term on the right-hand side models the interaction with the fixed wall, and the last term represents dissipation in the first particle. For a free boundary with a constant force, the third term in Supplementary Equation (1), which represents the interaction with the wall, is replaced with a constant force F_0. This yields the equation

$$\begin{aligned} m_1 \frac{d^2 u_1}{dt^2} = & A_{0,1} \left[\delta_{0,1} + u_0 - u_1\right]_+^{3/2} - A_{1,2} \left[\delta_{1,2} + u_1 - u_2\right]_+^{3/2} \\ & + F_0 - \frac{m_1}{\tau} \frac{du_1}{dt} \,. \end{aligned} \tag{2}$$

One can construe such a free boundary as an extreme case of a soft boundary.

We conduct numerical simulations using both boundary conditions. In Supplementary Figure 5c, we observe that the choice of boundary condition has a negligible effect for weak precompression, and the energy spreading exhibits similar superdiffusive behavior for both hard and soft boundaries. However, for progressively stronger precompression, the disparity between the two scenarios becomes larger. For hard boundaries, a significant amount of excitation energy is trapped near the boundary for a long time (compare the insets of Supplementary Figure 5c), so the exponent γ of m_2 suggests a trend towards subdiffusive spreading as one increases precompression. In contrast, for a soft boundary, localization is weaker and the energy spreads more rapidly. The resulting mean exponent γ asymptotically approaches a particular value (roughly 1.2) in the superdiffusive regime. This asymptotic value depends on the mass ratio of the heavy and light particles, similar to what has been

described for the bulk of a granular chain[4], and also on the initial excitation. Note that we estimate values of γ using a specified finite duration both in our numerical computations and in our experiments, so one can expect some discrepancies between these values and ones that are calculated over an infinite time horizon (i.e., asymptotic values as $t \to \infty$). However, in past work[3], it has been observed in numerical computations that the value of γ in an initial time period (of about 0.1–1 ms) seems to persist for a long time without significant changes.

Finally, comparing the results from Supplementary Figure 5c with those from Figure 5 of the main manuscript, we deduce that the boundary condition of our experimental setup corresponds to the hard boundary condition (i.e., the setup shown in Supplementary Figure 5a), based on the fact that $\gamma \leq 1$. This makes sense, given the clamped configuration of the first particle in the chain. (See the inset of Figure 1 of the main manuscript.)

SUPPLEMENTARY NOTE 7: COMPARISON OF M_2 BETWEEN SHORT AND LONG CHAINS.

We use numerical simulations to compare the exponent γ of the second moment m_2 of the kinetic energy between short chains (32 particles) and long chains (100 particles). We do this comparison for both velocity and displacement excitations. Previous studies reported that γ achieves a specific value[1,3,4] faster in time with velocity excitations than with displacement excitations[3,4]. In our simulations, we observe that the variation of the exponents is relatively small after about 0.1 ms, similar to the trend reported in 3. Therefore, we estimate the exponents during the time window $[0.1, 1]$ ms for the short chains and during the window $[0.1, 3]$ ms for the long chains using a least-squares fit. As we show in Supplementary Figures 6a (velocity excitations) and 6b (displacement excitations), the results from the short chains have minor discrepancies from those for the long chains, especially when one considers the large standard deviation (see the error bars) of the extracted exponents. In Supplementary Figure 6c, we show the statistical distribution of the exponents calculated using 100 chains of 32 particles for a velocity excitation (corresponding to the curve with blue squares in Supplementary Figure 6a). For weak precompression, the long chains have relatively large exponents for both velocity and displacement excitations. We expect that this observation is related to the detrapping of localized energy in the weakly nonlinear regime[4]. We also observe that the exponents for the displacement excitations are

smaller than corresponding ones for the velocity excitation. (Compare Supplementary Figures 6a and 6b.) This arises because a displacement excitation includes broadly-distributed frequencies, whereas a velocity excitation includes mostly low-frequency signals.

SUPPLEMENTARY NOTE 8: EFFECT OF DISSIPATION ON ENERGY SPREADING.

We investigate the effect of dissipation on energy spreading. For simplicity, we use linear damping, as indicated in the last term in Equation (3) of the main text. This is a common choice for incorporating dissipative effects in models of granular chains[3]. However, we note in passing that numerous models have been proposed to capture dissipative effects, and the issue of deriving a proper qualitative and quantitative incorporation of dissipation is an open problem[5]. In Supplementary Figure 7, we show the effect of the dissipation time scale τ on the exponent γ of the second moment m_2 of kinetic energy when we vary the static precompression F_0. When the effect of damping is significant ($\tau = 0.0004$), γ decreases slightly in the weakly and strongly nonlinear regimes. (Compare the blue squares with the red circles and green diamonds in Supplementary Figure 7.) However, we find that the global dissipation term does not significantly change the characteristics of energy spreading.

SUPPLEMENTARY NOTE 9: TESTING FOR PLASTICITY.

We also test for the possibility of plastic effects. First, we note that we did not observe any visible dents on the surface of the aluminum beads after repeated experiments. Additionally, the test data sets do not exhibit significant deviations from each other after repeated tests. To examine this possibility further, we numerically calculate (results not shown) the von Mises stress of the particles in contact. We find that although plastic deformation may happen inside the aluminum particles, it would have only a minor effect on the particle surfaces.

SUPPLEMENTARY NOTE 10: TYPES OF INITIAL CONDITIONS: VELOCITY AND DISPLACEMENT EXCITATIONS

We consider two types of initial conditions in our numerical simulations. Similar to simulations in prior work[3,4] for the bulk of a granular chain, in our examination of boundary-induced excitations, we conduct simulations with two types of initial conditions. We apply a velocity excitation that consists of an initial perturbation of the velocity of a single particle, with all other particles starting with zero velocity and all particles starting with zero displacement (see Supplementary Figure 6a). We also consider a displacement excitation of the position from equilibrium of a single particle (see Supplementary Figure 6b). In Supplementary Note 7, we used both types of initial conditions in our comparisons of short and long chains.

SUPPLEMENTARY NOTE 11: EFFECT OF THE MATERIAL OF THE FIRST PARTICLE IN A GRANULAR CHAIN ON ENERGY SPREADING.

We compare the exponents γ of the second moment m_2 of the kinetic energy for two types of chains: one with a light particle (aluminum particle) in the first ($i = 1$) spot and the other with a heavy particle (tungsten-carbide) in that spot. In Supplementary Figure 8, we show computational results for these two cases from numerical simulations of 100 chains with 100 particles each. For weak precompression, the two chains exhibit very different behaviors. However, as we consider progressively stronger precompression, the exponents of the two sets of chains approach the same value, and the energy in both sets is transported in a subdiffusive way. In the main text, we used light (i.e., aluminum) particles at the $i = 1$ spot to facilitate the transport of energy to the granular chain from the striker particle.

SUPPLEMENTARY REFERENCES

[1]P. K. Datta and K. Kundu, Energy transport in one-dimensional harmonic chains, Phys. Rev. B **51**, 6287–6295 (1995).

[2]T. W. Anderson and A. D. Darling, Asymptotic theory of certain "goodness-of-fit" criteria based on stochastic processes, Ann. Math. Stats. **23**, 193–212 (1952).

[3]A. J. Martínez, P. G. Kevrekidis, and M. A. Porter, Superdiffusive transport and energy localization in disordered granular crystals, Phys. Rev. E **93**, 022902 (2016).

[4]V. Achilleos, G. Theocharis, and Ch. Skokos, Energy transport in one-dimensional disordered granular solids, Phys. Rev. E **93**, 022903 (2016).

[5]C. Chong, M. A. Porter, P. G. Kevrekidis, and C. Daraio, Nonlinear coherent structures in granular crystals, J. Phys. Cond. Matt. **29**, 413003 (2017).